

Article

Spheroidization Behavior of Nano-Primary Silicon Induced by Neodymium under High-Current Pulsed Electron Beam Irradiation

Liang Hu [†], Kui Li [†], Bo Gao ^{*}, Ning Xu, Zhuang Liu, Yue Sun, Ying Zhang and Pengfei Xing

Key Laboratory for Ecological Metallurgy of Multimetallurgical Mineral (Ministry of Education), Northeastern University, Shenyang 110819, China; hss5566123@163.com (L.H.); Surflik@163.com (K.L.); xun0909@stumail.neu.edu.cn (N.X.); surfliuz@163.com (Z.L.); surfsuny@163.com (Y.S.); zhangyinghi@163.com (Y.Z.); xingpf@smm.neu.edu.cn (P.X.)

* Correspondence: gaob@smm.neu.edu.cn

[†] These authors contributed equally to this work.

Abstract: The spheroidization behavior of the nano-primary silicon phase induced by Nd under high-current pulsed electron beam (HCPEB) irradiation was investigated in this study. The study results revealed that, compared to the Al–17.5Si alloy, spheroidized nano-primary silicon phase emerged in the alloy’s HCPEB-irradiated surface layer due to the presence of Nd. Because Nd was abundantly enriched on the fast-growing silicon crystal plane, its surface tension was reduced under the extreme undercooling caused by HCPEB irradiation, causing the growth velocity of each crystal plane to be the same and spherical nanometers of silicon to appear. The spheroidization of nano-primary silicon phases occurred in the remelted layer. The microhardness test revealed that Nd could depress the microhardness of the Al matrix at the same number of pulses, but conversely increase the microhardness of the primary silicon phase, compared to the Al–17.5Si alloy. The tribological test showed that the presence of spherical nano-primary silicon could significantly improve the alloy’s tribological property.

Keywords: high-current pulsed electron beam; spheroidization of nano-primary silicon; Al–17.5Si–0.3Nd alloy; element diffusion effect; tribological property



Citation: Hu, L.; Li, K.; Gao, B.; Xu, N.; Liu, Z.; Sun, Y.; Zhang, Y.; Xing, P. Spheroidization Behavior of Nano-Primary Silicon Induced by Neodymium under High-Current Pulsed Electron Beam Irradiation. *Coatings* **2021**, *11*, 1408. <https://doi.org/10.3390/coatings11111408>

Academic Editor: Alessio Lamperti

Received: 21 October 2021

Accepted: 12 November 2021

Published: 19 November 2021

Publisher’s Note: MDPI stays neutral with regard to jurisdictional claims in published maps and institutional affiliations.



Copyright: © 2021 by the authors. Licensee MDPI, Basel, Switzerland. This article is an open access article distributed under the terms and conditions of the Creative Commons Attribution (CC BY) license (<https://creativecommons.org/licenses/by/4.0/>).

1. Introduction

Hypereutectic aluminum–silicon alloy has been widely used in components requiring weight reduction, such as aircraft and automobile fittings, particularly pistons, because of its advantages of low density, high specific strength, low thermal expansivity and good tribological property [1–3]. Among these alloys, A390 alloy (silicon content: 16–18 wt.%), with tensile strengths of 275 MPa and 102.1 MPa at room temperature and 300 °C, respectively, has been used in cylinders and pistons in key engine components [4,5]. However, due to a coarse primary silicon phase that splits the Al matrix, its application is limited. As a result, controlling the size and morphology of the primary silicon has always been one of the primary research interests in hypereutectic Al–Si alloys.

Chemical modification [6], ultrasonic vibration [7], electromagnetic stirring [8], and high pressure die casting [9] are currently the conventional modified primary silicon phase methods. Still, these methods can only refine the primary silicon size to the micron level. The high-current pulsed electron beam (HCPEB) is a new type of ultra-rapid solidification technology that can refine the size of the phase to nanometers [10]. As a new type of high-density energy source, HCPEB employs accelerated electrons as energy carriers. A large amount of energy rapidly (within microseconds) deposited in a thin layer of a material surface (~10 μm) generates a high-temperature gradient (~10⁷ K/m). Various physical processes (e.g., melting, vaporization and melt eruption) are also induced. Subsequently, the heat is rapidly dissipated via the chill effect of the material matrix during the rapid solidification process of the material surface. This yields metastable phases (e.g.,

supersaturated solid solution, nanocrystals and amorphous phases), which have excellent properties that are unattainable through conventional methods. Hao et al. [10,11] employed HCPEB technology to treat hypereutectic aluminum–silicon alloys to obtain nano-Si phases, including fine eutectic Si phases and nano-primary Si phases. Therefore, HCPEB is an excellent surface modification technique for obtaining nanoscale silicon phases via the rapid heating and cooling effects induced by the electron beam. In addition, some reports claim that the addition of trace elements (such as Na) can spheroidize primary silicon to a certain extent [12,13], but the modification effect is temporary, and the size remains relatively large. As long-lasting spheroidizing agents, rare-earth elements can significantly spheroidize the graphite phase in cast iron [14,15], thus introducing a novel approach to the spheroidization of the primary silicon phase (the phase has faceted growth similar to the graphite phase). Currently, there are few research reports on spheroidization of the primary silicon phase via HCPEB and rare-earth elements; therefore, this study focuses on studying the spheroidization behavior induced by Nd under HCPEB irradiation and proposes the corresponding spheroidization mechanism. Furthermore, the effect of spherical nano-silicon particles on the tribological property of the alloy surface was investigated.

2. Research Equipment

During this experiment, raw materials were smelted in a muffle furnace in a specific ratio, then cast and cut into cylindrical alloy specimens with $\phi = 10 \text{ mm} \times 10 \text{ mm}$. The nominal chemical components of alloy specimens were listed in Table 1. Various types of sandpapers (80, 240, 600, 800 and 1500 grit, Kovax, Tokyo, Japan) were used to grind, then 2.5 μm and 1.0 μm abrasive pastes (Sinomach, Zhengzhou, China) were used to polish the cut specimens. The polished specimen was then loaded into the “MMLAB-HOPE-I” (Dalian University of Technology, Dalian, China) device for HCPEB processing. The following test parameters were used: vacuum degree = $6 \times 10^{-3} \text{ Pa}$, acceleration voltage = 27 kV, energy density of = 5 J/cm^2 , pulse duration = 3 μs , target distance = 10 cm and number of pulses = 5, 15 and 25 pulses.

Table 1. The chemical components of alloy specimens.

Alloys	Al	Si	Nd
Al–17.5Si alloy	Bal.	17.5	-
Al–17.5Si–0.3 Nd alloy	Bal.	17.5	0.3

A field emission scanning electron microscope (FESEM) (Hitachi, S-4800, Tokyo, Japan) was used to examine the surface morphology of alloy specimens. The operating conditions of the SEM were the accelerating voltage of 15 kV and the working distance is 14.9 mm. A transmission electron microscope (TEM) (Tecnai, G20, Hillsboro, OR, USA) was used to observe metastable structures. The operating conditions of the TEM were the accelerating voltage of 200 kV, point resolution and line resolution of 0.248 nm and 0.144 nm, respectively. X-ray diffraction (Shimadzu XRD-7000, Kyoto, Japan) with a $\text{CuK}\alpha$ ($\lambda = 0.154 \text{ nm}$) was used to analyse the phase of alloy surfaces. A field emission electron microprobe (Jeol JXA-8530F, Tokyo, Japan) was used to analyse the elemental distribution in the cross-section of the HCPEB-irradiated alloy. This analysis was performed at an accelerating voltage of 30 kV, a working distance of 11 mm and a secondary electron image resolution of 3 nm. The microhardness of the alloy surfaces was gauged using a LECO LM247AT Vickers (San Jose, CA, USA) microhardness tester with a load of 10 g and a holding time of 10 s. For the Al matrix, four different positions were selected for measurement and the acquired microhardness results were subsequently averaged. For the primary Si phase, four positions adjacent to the phase centre were selected for measurement and the acquired microhardness values were similarly averaged. A multi-function tribometer (MTF-5000, Beijing Zhong Jingyi Technology Co. Ltd., Beijing, China) was used to conduct tribological testing on alloy surfaces. The relevant test parameters

were listed in Table 2. Three specimens were tested for each number of pulses, and the obtained values of the friction coefficient were averaged.

Table 2. Tribological test parameters of the alloy surface.

Ball Material Type	Working Time	Distance Traveled	Ball Pressure Force
Si ₃ N ₄	10 min	5 mm	1 N

3. Results and Discussion

3.1. Morphology Analysis

In previous studies [16,17], our group found that the unmodified Al–17.5Si alloy was refined into the nano-primary silicon phase because of the rapid heating and cooling effects of HCPEB. Rare earths, as an excellent modifier, can induce spheroidization of the silicon phase. Hence, the goal of this study is to realize Nd-induced spheroidization of the nano-primary silicon phase through HCPEB irradiation to improve the microhardness and tribological property of the alloy surface.

Figure 1 shows the formation of a nano-primary silicon phase formed on the surface of Al–17.5Si alloys without and with Nd using 25-pulsed irradiation. A nanometer primary silicon phase appears on the surface of an HCPEB-irradiated Al–17.5Si alloy, with an angular plate-like morphology (Figure 1a). However, the corner angle of the nano-primary silicon becomes obtuse after the addition of Nd, resulting in a spheroidized morphology (Figure 1b). This finding demonstrates that the morphology of the nano-primary silicon phase has undergone a fundamental transformation as a result of the Nd modification effect. The phase's relevant selected area electron diffraction pattern reveals that the spheroidized silicon phase exists as polycrystalline silicon. The corresponding XRD plot in Figure 1c shows that no new phase is formed, with Al and Si phases occurring as the main phases in HCPEB-irradiated Al–17.5Si alloy surfaces without and with Nd. The presence of Nd element is undetectable after HCPEB treatment, because the amount of this element is lower than the detection limit of XRD (5 wt.%). However, an electron probe microanalyzer EPMA investigation has revealed that Nd is uniformly distributed on the alloy surface because of the elemental diffusion effect induced by HCPEB [18]. Nd element dissolves in the Al matrix due to this diffusion, thereby forming a supersaturated Al-based solid solution. During the rapid heating process of the electron beam, Nd will diffuse along the direction of the reduced chemical gradient, eventually resulting in a uniform distribution of this element on the alloy surface. This diffusion behavior of Nd influences the spheroidization of nano-primary silicon (the corresponding spheroidization mechanism will be described in Section 3.2).

Figure 2 depicts the spheroidization process of nano-primary silicon. The primary silicon phase on the surface of the original alloy has a plate-like morphology (10–80 μm), as shown in Figure 2a. Following that, Si atomic clusters are formed in the surface-modified layer of the melted alloy due to HCPEB irradiation (Figure 2b). When the temperature drops, the atomic clusters grow to the critical nucleation size, lowering the system's free energy and allowing a stable silicon nucleus to form. The silicon phase is in the next growth stage and will be completely surrounded by Al (Figure 2c). As a result of the combined effect of Nd and the high degree of subcooling generated by HCPEB, the silicon phase further grows, and the growth mode of the primary silicon transitions from the original facet growth to the non-faceted growth, eventually growing into spherical nano-silicon (Figure 2d).

Figure 3 shows the cross-sectional composition of the 25-pulsed Al–17.5Si–0.3Nd alloy. As shown in Figure 3a, the thickness of the remelted layer of the alloy surface is 6.6 μm after the HCPEB treatment, and the nano-primary silicon undergoes spheroidization in this layer. The heat-affected zone lies below the remelted layer. Moreover, the microstructure of this area is consistent with the original microstructure of the alloy (Figure 2a), indicating that the modification effect of the alloy surface induced by the electron beam is limited

to the thin surface layer. Additionally, white rare-earth-rich intermetallic compounds occur around the primary silicon in the heat-affected zone, indicating an Nd enrichment in the original microstructure. However, Nd is uniformly distributed in the remelted layer (Figure 3d), indicating that the white rare-earth-rich intermetallic compound occurring in the original microstructure is dissolved by the electron beam irradiation. The irradiation process triggers the diffusion of Nd, and consequently the spheroidization of the nano-primary silicon phase. Similarly, Al and Si elements are homogeneously distributed in the remelted layer (Figure 3b,c). The homogeneous distribution of the elements in this layer contributes to improving the surface properties of the alloy.

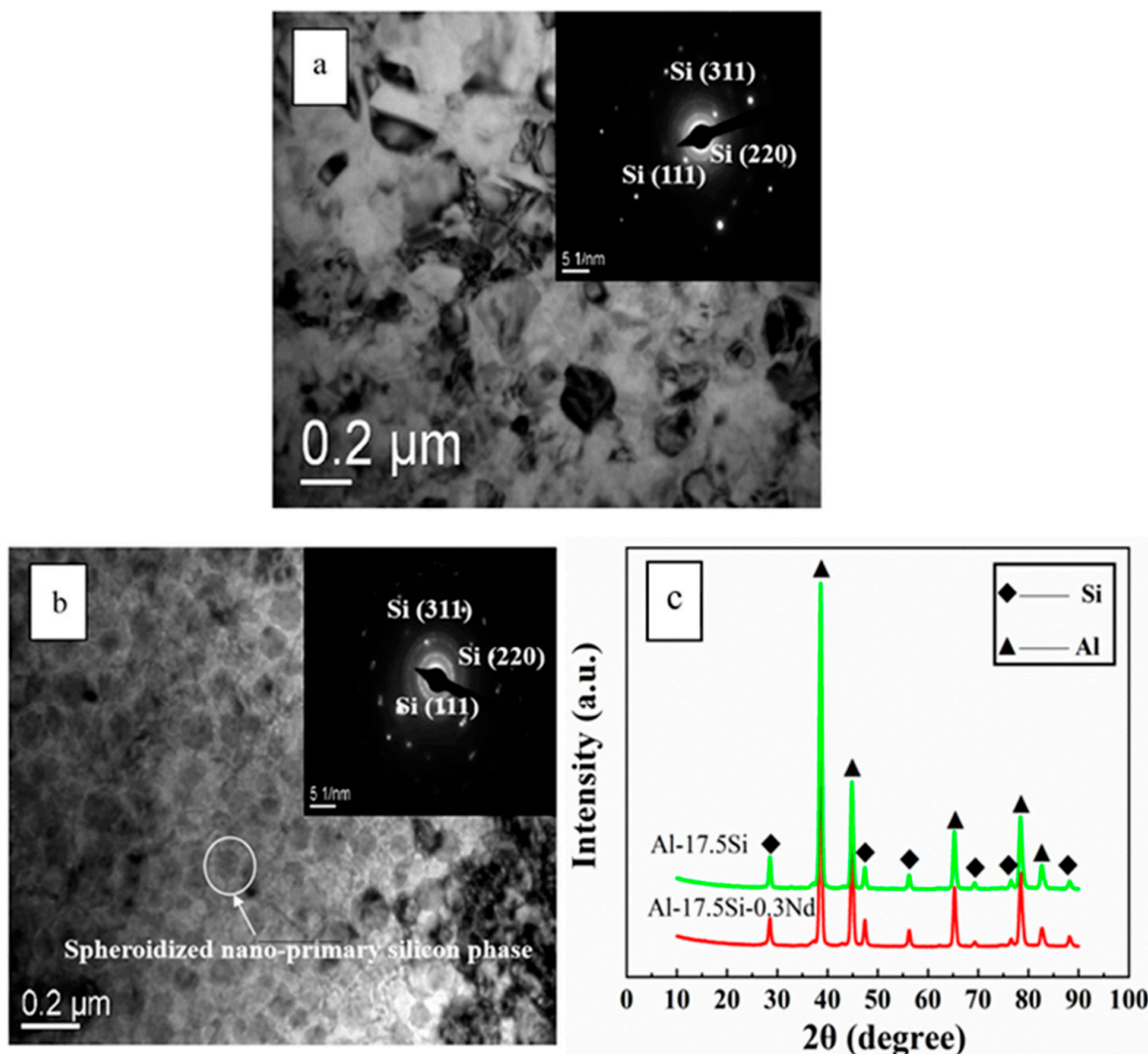


Figure 1. Nano-primary silicon phase formed in the surface layer of a 25-pulsed Al-17.5Si alloy without Nd and with Nd. (a) Unmodified nano-primary phase; (b) Spheroidized nano-primary silicon phase; (c) XRD plot corresponding to Figure 1a,b.

3.2. Spheroidization Mechanism of Nano-Primary Silicon Phase

The mechanism of the spheroidization of the primary silicon phase induced by Nd under the HCPEB irradiation is shown in Figure 4. In the first, Nd is distributed around the primary silicon in an Nd-rich intermetallic compound. The compound first melts under the HCPEB irradiation, and the primary silicon melts to form numerous small silicon clusters. Silicon nuclei are formed when the clusters reach the critical size for nucleation. Following

that, Nd diffuses around the silicon nucleus in the primary silicon due to the driving force of the elemental concentration gradient. During the subsequent rapid cooling process, most of the Nd is adsorbed on the crystal plane where the silicon nucleus growth is rapid, lowering the interfacial tension of the crystal plane and slowing the crystal surface growth. Because only a small amount of Nd is adsorbed on the slow-growing crystal plane, the growth velocity increases. Finally, the growth velocity of each crystal plane of the crystal nucleus tends to be the same, resulting in the formation of the spherical nano-primary silicon morphology.

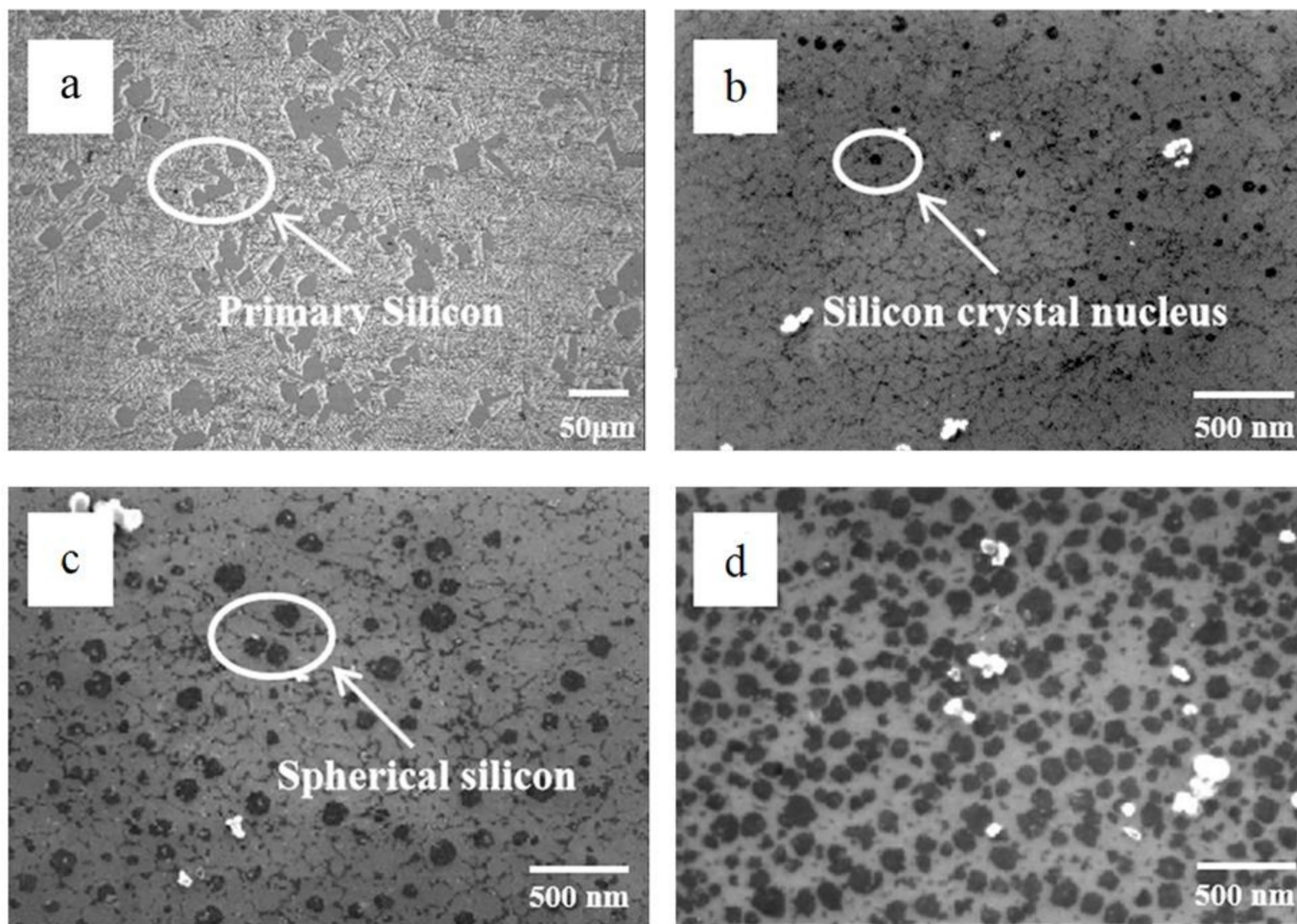


Figure 2. Spheroidization process of nano-primary silicon. (a) Initial stage, original specimen; (b) Nucleation stage; (c) Growth stage; (d) Formation stage.

3.3. Microhardness Analysis

The microhardness of the Al-17.5Si and Al-17.5Si-0.3Nd alloy specimens irradiated by HCPEB is presented in Figure 5. Compared to HCPEB-unirradiated alloy specimens, the microhardness of the Al matrix in the alloys increases as the number of pulses increases, which is interpreted as follows [11]: Firstly, the grain refinement of the Al matrix in the surface layer irradiated by HCPEB induces a fine-grain strengthening effect. Secondly, the Al-based supersaturated solid solution appears in the modified layer. Some of the Si atoms dissolve into the Al lattice under the rapid heating effect of the HCPEB, resulting in lattice distortion, thus forming a supersaturated solid solution, and inducing the solution strengthening effect. These two effects collectively enhance the microhardness of the Al matrix.

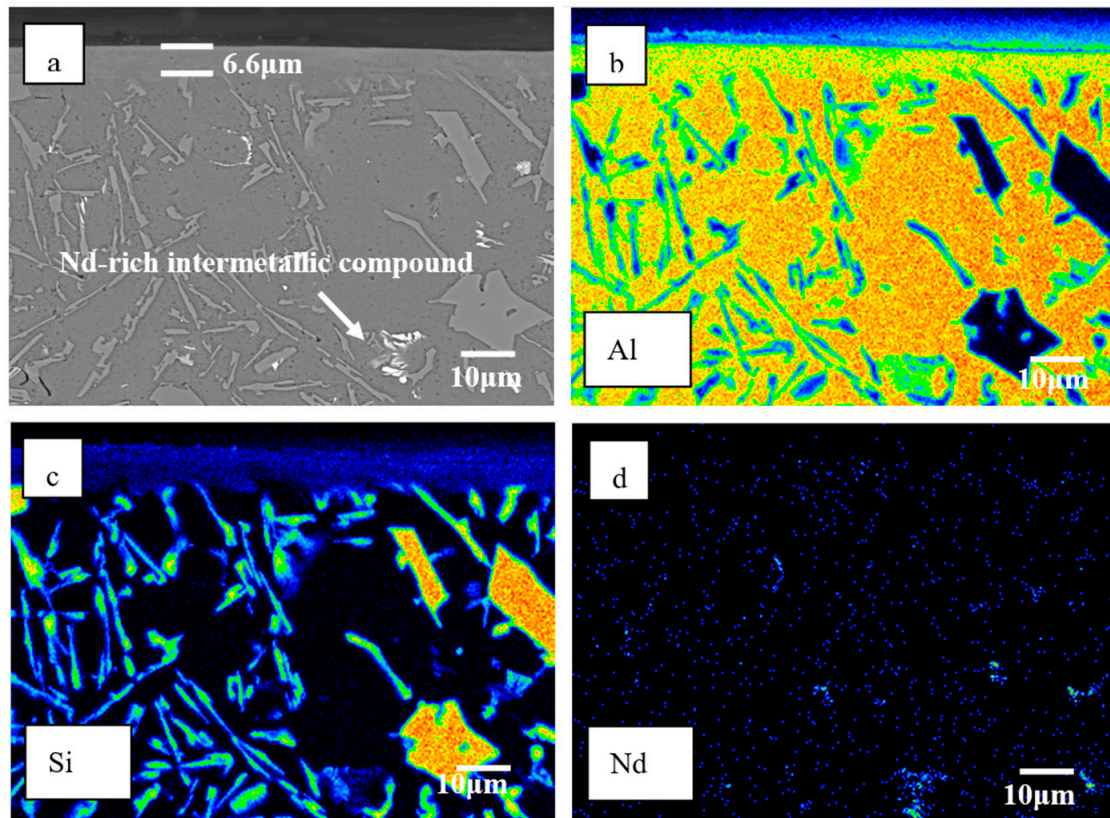


Figure 3. Cross-sectional composition distribution of a 25-pulsed Al-17.5Si-0.3Nd alloy (a) SEM image, BSE; (b) distribution of Al element; (c) distribution of Si element; (d) distribution of Nd element.

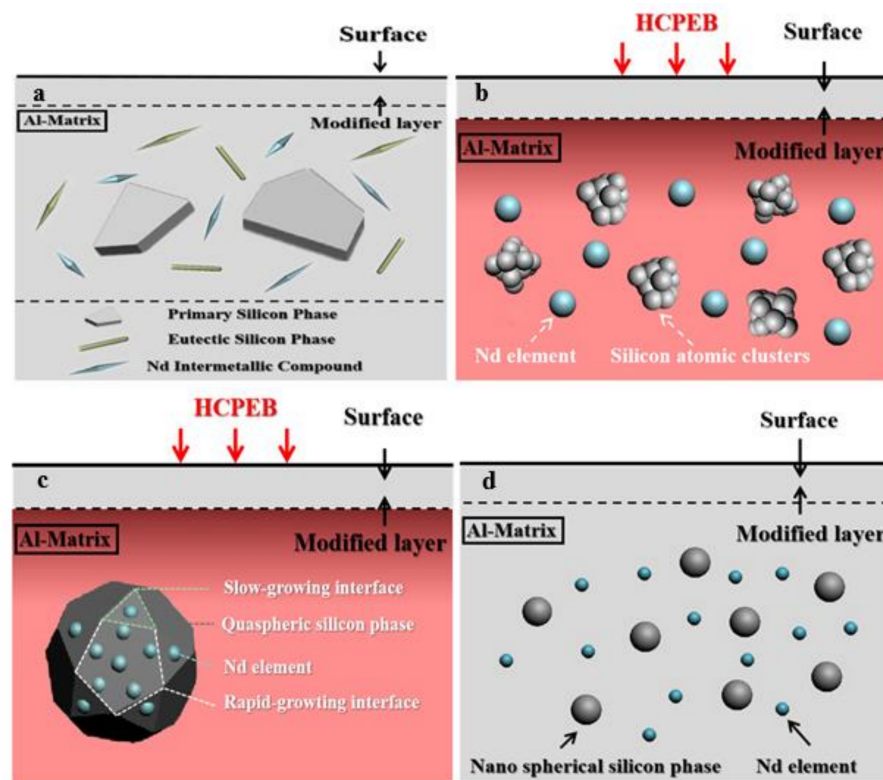


Figure 4. Schematic diagram of the spheroidization mechanism of the primary silicon phase induced by Nd under the HCPEB irradiation. (a) The initial stage; (b) The melting stage; (c) The spheroidizing stage; (d) The final stage.

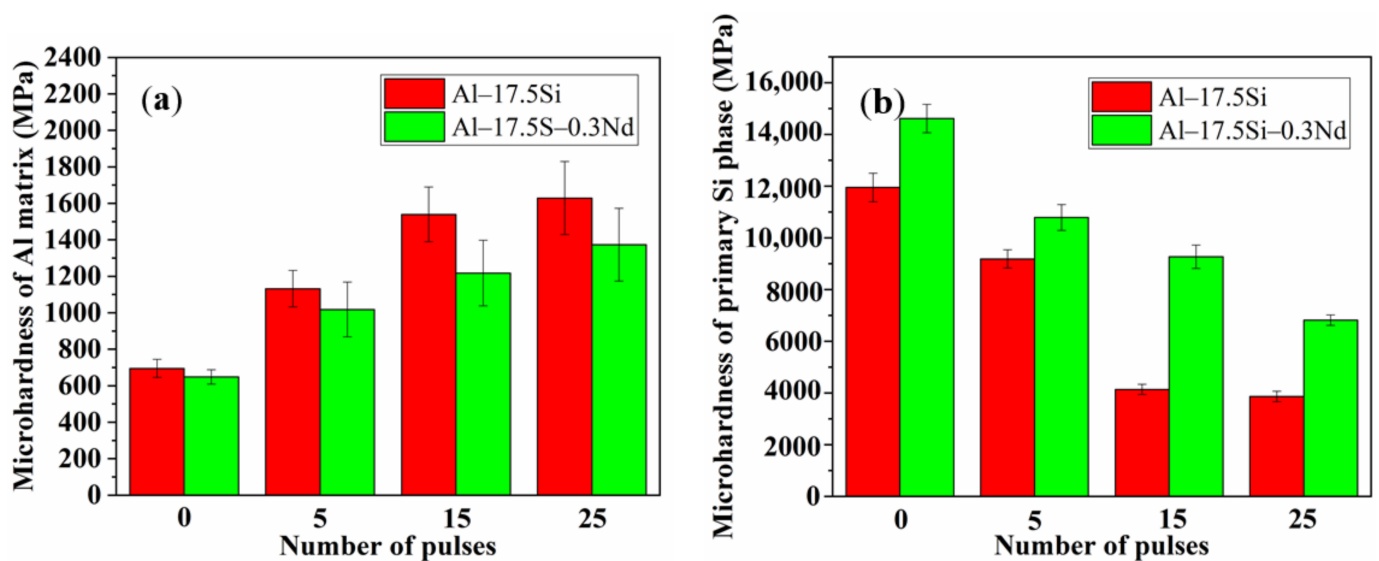


Figure 5. The relation between the microhardness of Al-17.5Si and Al-17.5Si-0.3Nd alloy surfaces and the number of pulses. (a) Al matrix; (b) Primary silicon phase.

Interestingly, Nd is shown in Figure 5a to suppress the microhardness of the Al matrix compared with that of the Al-17.5Si alloy specimens subjected to the same number of pulses. This suppressed microhardness is attributed to the toughening effect of Nd causing a sharp reduction in the amount of the hard Si phase in the Al matrix, thus decreasing the microhardness of the Al matrix. In comparison, the microhardness of the primary Si phase decreases with increasing number of pulses, compared to HCPEB-unirradiated alloy specimens (Figure 5b). This phenomenon is attributed to the Al gradually permeating into the primary Si phase because of the element diffusion effect induced by HCPEB and thereby decreasing the microhardness of the primary Si phase. Notably, however, Figure 5b shows that Nd conversely enhances the microhardness of the primary Si phase compared with that of the Al-17.5Si alloy specimen subjected to the same number of pulses because of the solid solution strengthening effect of Nd. A comparison of Figure 5a,b reveals that the microhardness of the Al matrix and primary Si phase for the Nd-incorporated alloys under HCPEB irradiation exhibits paradoxical behavior, which is attributed to the competition between the solid solution strengthening and toughening effects of the RE metal. In the case of the Al matrix, the toughening effect of Nd is dominant, thus contributing to a remarkable reduction of the Si content in the Al matrix and decreasing the microhardness of the phase. However, for the primary Si phase, the solid solution strengthening effect of Nd is dominant because of the high Si content in this phase, leading to an enhancement of the microhardness of the primary Si. The enhancement of the microhardness of the primary Si phase by Nd substantially improves the tribological properties of the alloy surface, as described in Section 3.4.

3.4. Tribological Properties

Figure 6 depicts the tribological property of two alloys before and after HCPEB treatments. The results show that HCPEB irradiation reduces the friction coefficient of the alloy surface and that adding the Nd element reduces this parameter even further. Additionally, Figure 7 shows the friction surface morphology of the two alloys before and after HCPEB treatment. The abrasion morphology of the alloy surface reveals that, in addition to the furrow wear marks, there are some large irregular strips of flaking pits on the abrasion surface of the original Al-17.5Si alloy (Figure 7a), which is attributed to spalling caused by the fracture of the primary silicon phase during repeated friction. The abrasion-resistant mechanism involves the typical furrow micro-cutting and fatigue spalling behavior. The craters induced by HCPEB cause small spalling pits on the abrasion

surface of the 25 pulse-processed Al-17.5Si alloy (Figure 7b). After 25 pulse treatments, no spalling pits are observed on the abrasion surface of the Al-17.5Si-0.3Nd alloy; only furrow abrasion marks are observed, and the abrasion surface is smoother, with wide and shallow abrasion furrows (Figure 7c), indicating that abrasive wear is the primary abrasion mechanism.

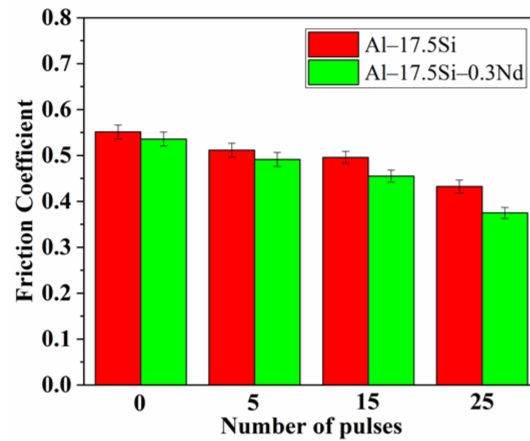


Figure 6. Friction-coefficient evolution of Al-17.5Si and Al-17.5Si-0.3Nd alloy surface with number of pulses.

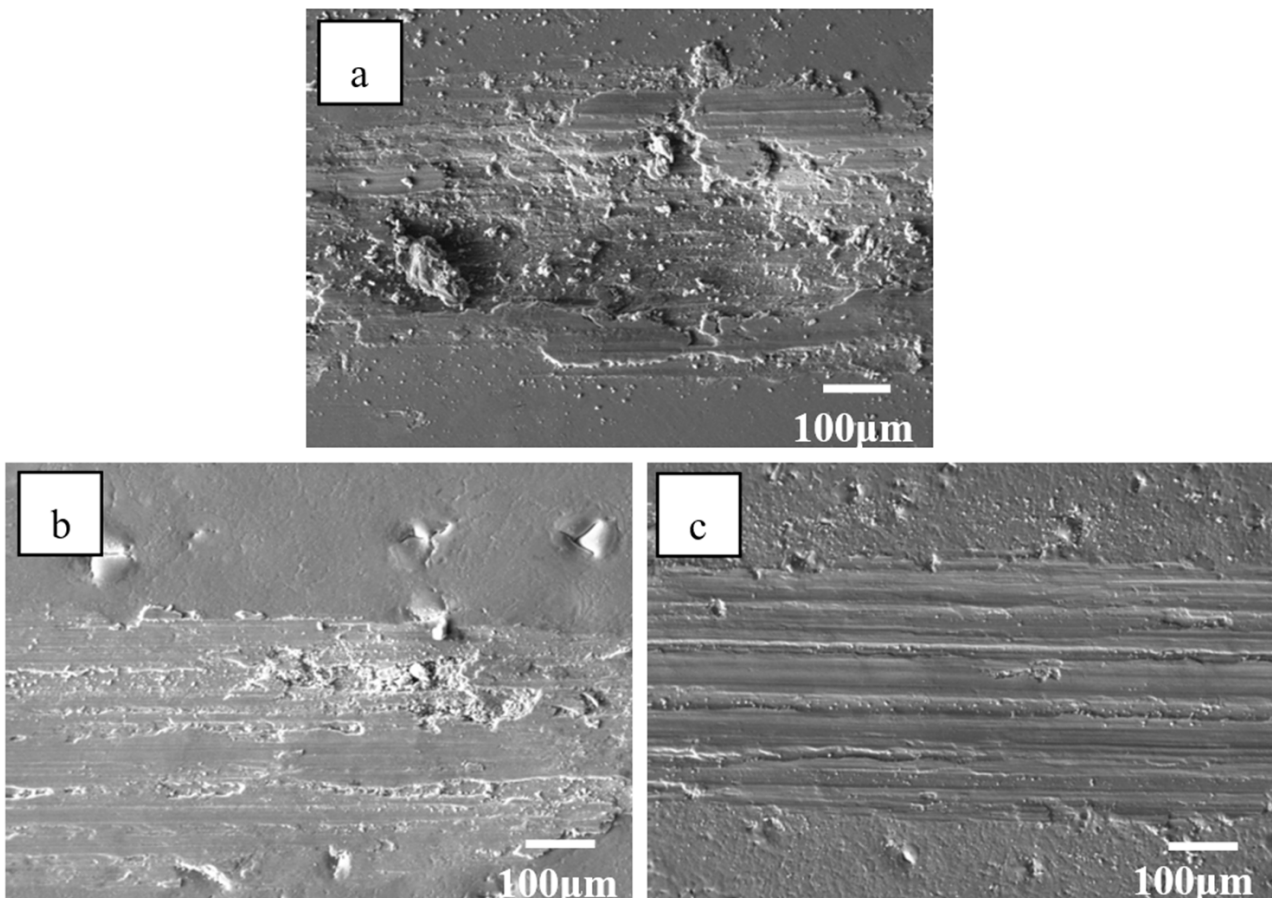


Figure 7. Friction surface morphology of Al-17.5Si and Al-17.5Si-0.3Nd alloys before and after HCPEB treatments. (a) Al-17.5Si alloy, original specimen; (b) Al-17.5Si alloy, 25 pulses; (c) Al-17.5Si-0.3Nd alloy, 25 pulses.

The following three factors contribute to improving the tribological property of an Al–17.5Si alloy modified by Nd and HCPEB:

1. The HCPEB treatment creates a large number of metastable structures on the alloy surface, which improves the microhardness and tribological property of the alloy surface.
2. The addition of Nd removes the craters that degrade friction performance [19]. Rare earths can purify a material, reduce the number of casting defects and lower the surface roughness of the material. Based on the formation mechanism of craters, the crater structure forms preferentially at sites such as impurity phases and casting defects. The rare earths could reduce the occurrence of these sites, causing a significant improvement in the uniformity of the original microstructure, thereby eliminating the crater structure. In addition, the polishing effect produced by the electron beam results in a substantial reduction of the crater structure on the alloy surface. This reduction leads to a decrease in the surface roughness of the alloy, and hence an increase in the contact area between the material and the friction pairs. Consequently, the material can withstand higher loads (than those withstood by the original material) and the tribological property of the alloy surface is improved.
3. The spheroidized primary silicon has no corner angle and is more closely combined with the matrix, making peeling off difficult and causing spalling abrasion. In addition, spherical primary silicon is evenly distributed as hard spots on the aluminum matrix to form an ideal anti-abrasion structure with good toughness and high strength.

4. Conclusions

The spheroidization behavior of nano-primary silicon phases induced by Nd during HCPEB processing was investigated in this study. The results demonstrated that the composite modification using Nd and HCPEB could refine the primary silicon phase while spheroidizing it, which was attributed to the abundantly enriched Nd on the fast-growing silicon crystal plane, reducing its surface tension under the extreme undercooling by the HCPEB treatment, causing the same growth velocity of each crystal plane and then leading to the formation of spherical nanometer silicon. The spheroidization of nano-primary silicon phases occurred in the remelted layer. The microhardness test revealed that Nd could depress the microhardness of the Al matrix at the same number of pulses, but conversely increase the microhardness of the primary silicon phase, which was attributed to the competition between the solid solution strengthening and toughening effects of Nd. The tribological test revealed that spherical nano-primary silicon could significantly improve the alloy's tribological property.

Author Contributions: Writing-original draft, L.H.; methodology, L.H.; software, K.L. and Y.S.; validation, K.L. and Y.S.; supervision, B.G. and P.X.; funding acquisition, B.G. and P.X.; data curation, N.X.; visualization, N.X. and Y.Z.; writing-review and editing, Z.L.; formal analysis, Z.L.; investigation, Y.Z. All authors have read and agreed to the published version of the manuscript.

Funding: This work was financially supported by the Fundamental Research Funds for the Central Universities (N182502042) and LiaoNing Revitalization Talents Program (XLYC1902105).

Institutional Review Board Statement: Not applicable.

Informed Consent Statement: Not applicable.

Data Availability Statement: Data can be requested from the corresponding author at request.

Conflicts of Interest: The authors declare no conflict of interest.

References

1. Ganiger, B.; Chandrashekharaiah, T.; Prasad, T.; Kabadi, V. Studies on Relationship between Wear Behaviour and Microstructure of a Hypereutectic Al–Si Alloy. *Mater. Today Proc.* **2018**, *5*, 25165–25173. [[CrossRef](#)]
2. Jiang, Q.C.; Xu, C.L.; Lu, M.; Wang, H.Y. Effect of new Al–P–Ti–TiC–Y Modifier on Primary Silicon in Hypereutectic Al–Si Alloys. *Mater. Lett.* **2005**, *59*, 624–628. [[CrossRef](#)]

3. Li, Q.; Xia, T.; Lan, Y.; Zhao, W.; Fan, L.; Li, P. Effect of Rare Earth Cerium Addition on the Microstructure and Tensile Properties of Hypereutectic Al–20% Si alloy. *J. Alloys Compd.* **2013**, *562*, 25–32. [[CrossRef](#)]
4. Damavandi, E.; Nourouzi, S.; Rabiee, S.M.; Jamaati, R. Effect of ECAP on Microstructure and Tensile Properties of A390 Aluminum Alloy. *Trans. Nonferr. Met. Soc. China* **2019**, *29*, 931–940. [[CrossRef](#)]
5. Li, P.; Li, Y.; Wu, Y.; Ma, G.; Liu, X. Distribution of TiB₂ Particles and Its Effect on the Mechanical Properties of A390 Alloy. *Mater. Sci. Eng. A* **2012**, *546*, 146–152. [[CrossRef](#)]
6. Jeon, J.; Shin, J.; Bae, D. Si Phase Modification on the Elevated Temperature Mechanical Properties of Al–Si Hypereutectic Alloys. *Mater. Sci. Eng. A* **2019**, *748*, 367–370. [[CrossRef](#)]
7. Feng, H.K.; Yu, S.R.; Li, Y.L.; Gong, L.Y. Effect of Ultrasonic Treatment on Microstructures of Hypereutectic Al–Si Al-Loy. *J. Mater. Process. Technol.* **2008**, *208*, 330–335. [[CrossRef](#)]
8. He, Y.F.; Yang, X.; Bao, Y.; Li, S.Y.; Chen, Z.J.; Ma, W.H.; Lv, G.Q. Effects of Silicon Content on the Separation and Purification of Primary Silicon from Hypereutectic Aluminum–Silicon Alloy by Alternating Electromagnetic Directional Solidification. *Sep. Purif. Technol.* **2019**, *219*, 25–32. [[CrossRef](#)]
9. Jiao, X.; Wang, J.; Liu, C.; Guo, Z.; Tong, G.; Ma, S.; Bi, Y.; Zhang, Y.; Xiong, S. Characterization of High-Pressure Die-Cast Hypereutectic Al–Si Alloys Based on Microstructural Distribution and fracture morphology. *J. Mater. Sci. Technol.* **2019**, *35*, 1099–1107. [[CrossRef](#)]
10. Hao, Y.; Gao, B.; Tu, G.F.; Wang, Z.; Hao, S.Z. Influence of High Current Pulsed Electron Beam (HCPB) Treatment on Wear Resistance of Hypereutectic Al–17.5Si and Al–20Si Alloys. *Mater. Sci. Forum* **2011**, *675–677*, 693–696. [[CrossRef](#)]
11. Hao, Y.; Gao, B.; Tu, G.; Li, S.; Hao, S.; Dong, C. Surface Modification of Al–20Si Alloy by High Current Pulsed Electron Beam. *Appl. Surf. Sci.* **2011**, *257*, 3913–3919. [[CrossRef](#)]
12. Fatahalla, N.; Hafiz, M.; Abdulkhalek, M. Effect of Microstructure on the Mechanical Properties and Fracture of Commercial Hypoeutectic Al–Si Alloy Modified with Na, Sb and Sr. *J. Mater. Sci.* **1999**, *34*, 3555–3564. [[CrossRef](#)]
13. Li, J.H.; Barrirero, J.; Engstler, M.; Aboufadel, H.; Mücklich, F.; Schumacher, P. Nucleation and Growth of Eutectic Si in Al–Si Alloys with Na Addition. *Met. Mater. Trans. A* **2014**, *46*, 1300–1311. [[CrossRef](#)]
14. Choi, J.; Kim, J.; Choi, C.; Rohatgi, P. Effect of Rare Earth Element on Microstructure Formation and Mechanical Properties of Thin Wall Ductile Iron Castings. *Mater. Sci. Eng. A* **2004**, *383*, 323–333. [[CrossRef](#)]
15. Wang, L.; Guo, E.; Chen, H.; Wang, J.; Li, D. Effects of Light and Heavy Rare Earths on Anti-Degradation of Nodular Cast Iron. *J. Rare Earths* **2006**, *24*, 103–107. [[CrossRef](#)]
16. Hu, L.; Gao, B.; Lv, J.K.; Hao, Y.; Tu, G.F.; Hao, S.Z.; Dong, C. The Metastable Structure of Hypereutectic Al–17.5Si Alloy Surface Induced by High Current Pulsed Electron Beam. *Mater. Res. Innov.* **2015**, *19*, S320–S324. [[CrossRef](#)]
17. Hu, L.; Gao, B.; Lv, J.K.; Sun, S.C.; Hao, Y.; Tu, G.F. Halo Evolution of Hypereutectic Al–17.5Si Alloy Treated with High-Current Pulsed Electron Beam. *J. Nanomater.* **2015**, *16*, 247. [[CrossRef](#)]
18. Hu, L.; Gao, B.; Zhu, G.L.; Hao, Y.; Sun, S.C.; Tu, G.F. The Effect of Neodymium on the Microcracks Generated on the Al–17.5Si Alloy Surface by High Current Pulsed Electron Beam. *Appl. Surf. Sci.* **2016**, *364*, 490–497. [[CrossRef](#)]
19. Li, K.; Gao, B.; Xu, N.; Sun, Y.; Denisov, V.V.; Hu, L. The Influence of Neodymium Element on the Crater Structure Formed on Al–17.5Si Alloy Surface Processed by High-Current Pulsed Electron Beam. *Coatings* **2020**, *10*, 922. [[CrossRef](#)]